

Control Allocation and Quantization of a GEO Satellite with 4DOF Gimbaled Thruster Booms

Caverly, Ryan; Di Cairano, Stefano; Weiss, Avishai

TR2020-008 January 15, 2020

Abstract

This paper presents a control allocation and thruster quantization method to simultaneously perform station keeping, attitude control, and momentum management of a geostationary Earth orbit (GEO) satellite equipped with two electric thrusters mounted on gimbaled booms, each with four degrees-of-freedom (DOFs). A modified version of a previously-developed model predictive control (MPC) policy is used to generate an optimal body force and torque that is then allocated and quantized before being implemented on the satellite. The novel control allocation method optimally solves for boom gimbal angles and thruster magnitudes that produce a force and torque that best match the force and torque calculated using the MPC policy. The quantization scheme then optimizes the on-off times of each thruster to minimize error in the predicted satellite states due to quantization. Numerical simulation results are presented that illustrate the performance of the proposed control formulation and highlight the fuel consumed due to the individual control allocation and thrust quantization stages.

AAS/AIAA Space Flight Mechanics Meeting

This work may not be copied or reproduced in whole or in part for any commercial purpose. Permission to copy in whole or in part without payment of fee is granted for nonprofit educational and research purposes provided that all such whole or partial copies include the following: a notice that such copying is by permission of Mitsubishi Electric Research Laboratories, Inc.; an acknowledgment of the authors and individual contributions to the work; and all applicable portions of the copyright notice. Copying, reproduction, or republishing for any other purpose shall require a license with payment of fee to Mitsubishi Electric Research Laboratories, Inc. All rights reserved.

Control Allocation and Quantization of a GEO Satellite with 4DOF Gimbaled Thruster Booms

Ryan J. Caverly*

University of Minnesota, Minneapolis, MN 55455, USA

Stefano Di Cairano[†]

Avishai Weiss[‡]

Mitsubishi Electric Research Laboratories, Cambridge, MA 02139, USA

This paper presents a control allocation and thruster quantization method to simultaneously perform station keeping, attitude control, and momentum management of a geostationary Earth orbit (GEO) satellite equipped with two electric thrusters mounted on gimbaled booms, each with four degrees-of-freedom (DOFs). A modified version of a previously-developed model predictive control (MPC) policy is used to generate an optimal body force and torque that is then allocated and quantized before being implemented on the satellite. The novel control allocation method optimally solves for boom gimbal angles and thruster magnitudes that produce a force and torque that best match the force and torque calculated using the MPC policy. The quantization scheme then optimizes the on-off times of each thruster to minimize error in the predicted satellite states due to quantization. Numerical simulation results are presented that illustrate the performance of the proposed control formulation and highlight the fuel consumed due to the individual control allocation and thrust quantization stages.

I. Introduction

Low-thrust electric propulsion has recently been proposed as an efficient alternative to chemical propulsion for the station keeping of geostationary Earth orbit (GEO) satellites.¹ Due to a lower thrust magnitude than chemical propulsion, electric propulsion requires more frequent, near-continuous thruster firings, which complicates the planning of station keeping maneuvers. To address this challenge, a number of closed-loop autonomous feedback control methods have been developed.^{2–15} In particular, model predictive control (MPC) has been used for simultaneous station keeping, attitude control, and momentum management with electric propulsion.^{11–15} MPC is well-suited for this problem, as it is capable of handling multiple control objectives and multiple state and control constraints.¹⁶ Increasingly complex thruster configurations are considered in Refs. 11–15, beginning with twelve fixed thrusters in Ref. 11, four anti-nadir-facing thrusters in Ref. 12, and four thrusters mounted on two booms, each actuated by a single gimbal angle in Refs. 13–15. By increasing the complexity of the thruster configurations, fewer thrusters are needed to maintain or improve performance (e.g., a reduction in Δv or on-off thruster cycles), ultimately reducing satellite costs. However, increased thruster configuration complexity necessitates novel, more advanced control strategies or significant extensions to existing control strategies.

The research presented in this paper builds off the work of Refs. 14, 15 by considering a satellite equipped with a more complex thruster-boom assembly. In particular, the satellite features two electric thrusters, each mounted on a gimbaled boom with four degrees-of-freedom (DOFs), which is comparable to the Deployable Thruster Module Assembly (DTMA) of the Airbus Eurostar E3000 satellite.¹⁷ This leads to a substantially more complex control formulation than in Refs. 14, 15, which considered four electric thrusters mounted on two gimbaled booms, each with a single DOF. The motivation for a more complex boom assembly is that

*Assistant Professor (rcaverly@umn.edu), Department of Aerospace Engineering and Mechanics, AIAA Member.

[†]Distinguished Research Scientist (dicairano@merl.com), AIAA Member.

[‡]Principal Research Scientist (weiss@merl.com), AIAA Member.

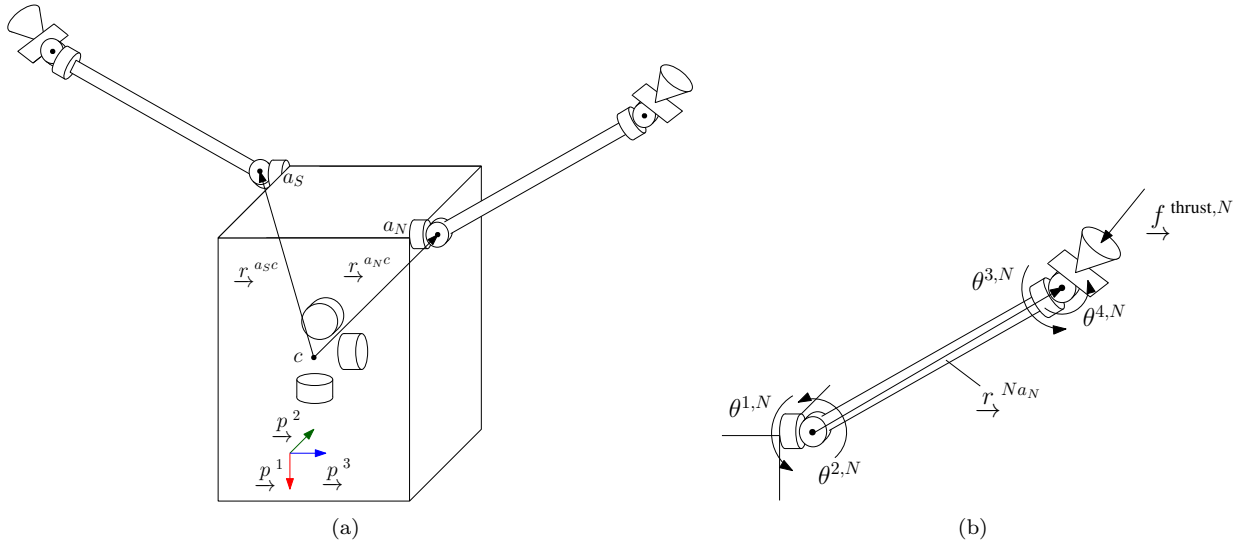


Figure 1. Schematic of (a) the spacecraft including three axisymmetric reaction wheels and two electric thrusters, and (b) the detailed North-facing boom-thruster assembly.

additional boom DOFs can potentially lead to improved performance even if the spacecraft is equipped with only two thrusters. The novel contribution of this paper is the development of optimal control allocation and thruster quantization methods that allow for a previously-developed MPC policy^{14,15} to be used for simultaneous station keeping, attitude control, and momentum management of a GEO satellite with two electric thrusters mounted on 4 DOF gimbaled booms. The optimal control allocation and thruster quantization methods are solved as nonlinear optimization problems, yielding optimally-allocated boom gimbal angles and optimal on-off thruster times at each time step.

A. Notation

The following notation is used throughout the paper. A reference frame \mathcal{F}_a is defined by a set of three orthonormal dextral basis vectors, $\{\underline{a}^1, \underline{a}^2, \underline{a}^3\}$. An arbitrary physical vector, denoted as \underline{v} , is resolved in \mathcal{F}_a as \mathbf{v}_a , where $\mathbf{v}_a^T = [v_{a1} \ v_{a2} \ v_{a3}]$ and $\underline{v} = v_{a1} \underline{a}^1 + v_{a2} \underline{a}^2 + v_{a3} \underline{a}^3$. The mapping between a physical vector resolved in different reference frames is given by the direction cosine matrix (DCM) $\mathbf{C}_{ba} \in SO(3)$, where $SO(3) = \{\mathbf{C} \in \mathbb{R}^{3 \times 3} \mid \mathbf{C}^T \mathbf{C} = \mathbf{I}, \det(\mathbf{C}) = +1\}$ and \mathbf{I} is the identity matrix. For example, $\mathbf{v}_b = \mathbf{C}_{ba} \mathbf{v}_a$, where \mathbf{v}_b is \underline{v} resolved in \mathcal{F}_b and \mathbf{C}_{ba} represents the attitude of \mathcal{F}_b relative to \mathcal{F}_a . Principle rotations about the \underline{a}^i axis by an angle α are denoted as $\mathbf{C}_{ba} = \mathbf{C}_i(\alpha)$. The cross, uncross, and anti-symmetric projection operators used throughout this paper are defined as follows. The cross operator, $(\cdot)^\times : \mathbb{R}^3 \rightarrow \mathfrak{so}(3)$, is defined as

$$\mathbf{a}^\times = -\mathbf{a}^{\times T} = \begin{bmatrix} 0 & -a_3 & a_2 \\ a_3 & 0 & -a_1 \\ -a_2 & a_1 & 0 \end{bmatrix},$$

where $\mathbf{a}^T = [a_1 \ a_2 \ a_3]$ and $\mathfrak{so}(3) = \{\mathbf{S} \in \mathbb{R}^{3 \times 3} \mid \mathbf{S} + \mathbf{S}^T = \mathbf{0}\}$. The uncross operator, $(\cdot)^\vee : \mathfrak{so}(3) \rightarrow \mathbb{R}^3$, is defined as $\mathbf{A}^\vee = [a_1 \ a_2 \ a_3]^T$, where $\mathbf{A} = \mathbf{a}^\times$. The anti-symmetric projection operator $\mathcal{P}_a(\cdot) : \mathbb{R}^{3 \times 3} \rightarrow \mathfrak{so}(3)$, is given by $\mathcal{P}_a(\mathbf{U}) = \frac{1}{2} (\mathbf{U} - \mathbf{U}^T)$, for all $\mathbf{U} \in \mathbb{R}^{3 \times 3}$. The physical vector describing the position of a point p relative to a point q is given by \underline{r}^{pq} . Similarly, the angular velocity of \mathcal{F}_b relative to \mathcal{F}_a is given by $\underline{\omega}^{ba}$.

B. Problem Statement and Control Architecture

Consider the satellite shown in Figure 1, which consists of a rigid bus equipped with three axisymmetric reaction wheels and two electric thrusters mounted on gimbaled booms. The objective of this work is to modify and extend the MPC policies developed in Refs. 14, 15 for a satellite equipped with four thrusters mounted on booms with a single gimbal angle to handle the propulsion configuration of a satellite equipped

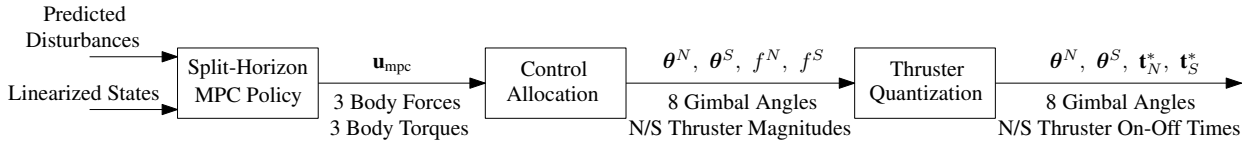


Figure 2. Block diagram of the three stages that make up the proposed control architecture.

with two thrusters mounted on booms with four gimbal angles. Similarly to Refs. 14,15, the control objective is to minimize fuel consumption while ensuring that GEO station keeping and attitude constraints are satisfied, angular momentum of the reaction wheels is unloaded, and the thrusters operate within their operational limits.

To solve this problem, the split-horizon MPC policies found in Refs. 14,15 are adapted. At each time step, the following three tasks are performed sequentially:

1. A split-horizon MPC policy calculates the optimal body force and torque to apply to the spacecraft.
2. Control allocation determines the optimal combination of thruster gimbal angles and thrust magnitudes at the current time step.
3. Thruster quantization determines the optimal on and off times for each thruster within the current time step.

This proposed control architecture is presented in block-diagram for in Figure 2. The model of the satellite is described in Section II. A brief description of the split-horizon MPC policy is found in Section III, while the control allocation and thruster quantization stages are described in Section IV.

II. Satellite Model

The satellite dynamic model considered in this paper is based on the configuration shown in Figure 1 and is derived based on the procedure in Ref. 13. The Earth-centered inertial (ECI) frame is defined as \mathcal{F}_g . The reference frame \mathcal{F}_p is aligned with the spacecraft bus, where nominally \underline{p}^1 points towards the Earth and \underline{p}^2 points North. The angular velocity of \mathcal{F}_p relative to \mathcal{F}_g is $\underline{\omega}^{pg}$ and the DCM describing the attitude of the spacecraft (i.e., frame \mathcal{F}_p) relative to \mathcal{F}_g is \mathbf{C}_{pg} . The center of mass of the spacecraft is denoted by point c in Figure 1(a). The position of the spacecraft center of mass relative to a point w at the center of the Earth is given by \underline{r}^{cw} . The equations of motion of the satellite are¹³

$$\ddot{\mathbf{r}}_g^{cw} = -\mu \frac{\mathbf{r}_g^{cw}}{\|\mathbf{r}_g^{cw}\|^3} + \mathbf{a}_g^p + \frac{1}{m_B} \mathbf{C}_{pg}^T \mathbf{f}_p^{\text{thrust}}, \quad (1a)$$

$$\mathbf{J}_p^{\mathcal{B}c} \dot{\underline{\omega}}_p^{pg} = -\underline{\omega}_p^{pg \times} (\mathbf{J}_p^{\mathcal{B}c} \underline{\omega}_p^{pg} + \mathbf{J}_s \dot{\underline{\gamma}}) - \mathbf{J}_s \underline{\eta} + \underline{\tau}_p^p + \underline{\tau}_p^{\text{thrust}}, \quad (1b)$$

$$\dot{\mathbf{C}}_{pg} = -\underline{\omega}_p^{pg \times} \mathbf{C}_{pg}, \quad (1c)$$

$$\dot{\underline{\gamma}} = \underline{\eta}, \quad (1d)$$

where m_B is the mass of the spacecraft, $\mathbf{J}_p^{\mathcal{B}c}$ is the moment of inertia of the spacecraft relative to point c and resolved in \mathcal{F}_p , $\underline{\gamma}^T = [\gamma_1 \ \gamma_2 \ \gamma_3]$ are the reaction wheel angles, $\underline{\eta}$ is the acceleration of the reaction wheels, \mathbf{J}_s is the moment of inertia of the reaction wheel array, $\mathbf{f}_p^{\text{thrust}}$ is the force produced by the thrusters, $\underline{\tau}_p^{\text{thrust}}$ is the torque produced by the thrusters, \mathbf{a}_g^p includes acceleration perturbations, and $\underline{\tau}_p^p$ includes torque perturbations.

The satellite is equipped with two electric thrusters mounted on booms that nominally point North and South, as shown in Figure 1. The direction of each thruster boom is governed by four gimbal angles, written collectively as $\underline{\theta}^{N^T} = [\theta^{1,N} \ \theta^{2,N} \ \theta^{3,N} \ \theta^{4,N}]$ for the North boom and $\underline{\theta}^{S^T} = [\theta^{1,S} \ \theta^{2,S} \ \theta^{3,S} \ \theta^{4,S}]$ for the South boom. The thruster booms are arranged such that thrust magnitudes of f^N in the North boom and

f^S in the South boom generate the following forces resolved in \mathcal{F}_p .

$$\mathbf{f}_p^{\text{thrust},N} = \mathbf{C}_{Np}^T \begin{bmatrix} 0 \\ 0 \\ -f^N \end{bmatrix}, \quad \mathbf{f}_p^{\text{thrust},S} = \mathbf{C}_{Sp}^T \begin{bmatrix} 0 \\ 0 \\ -f^S \end{bmatrix},$$

where

$$\begin{aligned} \mathbf{C}_{Np} &= \mathbf{C}_2(\theta^{4,N})\mathbf{C}_3(\theta^{3,N})\mathbf{C}_2(\theta^{2,N})\mathbf{C}_3(\theta^{1,N})\mathbf{C}_3(\pi), \\ \mathbf{C}_{Sp} &= \mathbf{C}_2(\theta^{4,S})\mathbf{C}_3(\theta^{3,S})\mathbf{C}_2(\theta^{2,S})\mathbf{C}_3(\theta^{1,S})\mathbf{C}_1(\pi)\mathbf{C}_3(\pi). \end{aligned}$$

The total force acting on the spacecraft is $\mathbf{f}_p^{\text{thrust}} = \mathbf{f}_p^{\text{thrust},N} + \mathbf{f}_p^{\text{thrust},S}$. The torque generated by the thrusters relative to the spacecraft's center of mass resolved in \mathcal{F}_p is $\boldsymbol{\tau}_p^{\text{thrust}} = \mathbf{r}_p^{Nc \times} \mathbf{f}_p^{\text{thrust},N} + \mathbf{r}_p^{Sc \times} \mathbf{f}_p^{\text{thrust},S}$, where

$$\mathbf{r}_p^{Nc} = \mathbf{C}_3^T(\pi)\mathbf{C}_3^T(\theta^{1,N})\mathbf{C}_2^T(\theta^{2,N}) \begin{bmatrix} 0 \\ 0 \\ \ell_N \end{bmatrix} + \mathbf{r}_p^{a_{Nc}}, \quad \mathbf{r}_p^{Sc} = \mathbf{C}_3^T(\pi)\mathbf{C}_1^T(\pi)\mathbf{C}_3^T(\theta^{1,S})\mathbf{C}_2^T(\theta^{2,S}) \begin{bmatrix} 0 \\ 0 \\ \ell_S \end{bmatrix} + \mathbf{r}_p^{a_{Sc}},$$

ℓ_N and ℓ_S are the lengths of the North and South booms, and $\mathbf{r}_p^{a_{Nc}}$ and $\mathbf{r}_p^{a_{Sc}}$ are the positions of the North and South boom attachment points relative to the spacecraft's center of mass resolved in \mathcal{F}_p .

III. MPC Formulation

This section presents a brief overview of the implemented MPC policy, which is largely based on the split-horizon policy introduced in Refs. 14, 15. The major difference with the MPC policies in Refs. 14, 15 is that the inputs to the state-space model are the net force and net torque acting on the spacecraft body, as opposed to the forces being generated by each thruster. This difference is due to the increased number of DOFs in the propulsion system, which makes it more effective to plan for forces and torques directly, and then allocate them to the thrusters by resolving the gimbal angles and thrust magnitudes.

A. Inner-Loop Attitude Controller

Attitude control of the spacecraft is performed using reaction wheels and the control law from Ref. 18. The control law models the disturbance torque acting on the spacecraft as the output of the LTI system $\dot{\mathbf{x}}_{\text{dist}} = \mathbf{A}_{\text{dist}}\mathbf{x}_{\text{dist}}$, $\boldsymbol{\tau}_p^p = \mathbf{C}_{\text{dist}}\mathbf{x}_{\text{dist}}$. An observer of the form $\dot{\hat{\mathbf{x}}}_{\text{dist}} = \mathbf{A}_{\text{dist}}\hat{\mathbf{x}}_{\text{dist}} + \mathbf{B}_{\text{dist}}\mathbf{u}_{\text{dist}}$ and $\hat{\boldsymbol{\tau}}_p^p = \mathbf{C}_{\text{dist}}\hat{\mathbf{x}}_{\text{dist}}$ is used to estimate the disturbance torque, where $\hat{\boldsymbol{\tau}}_p^p$ is the estimate of $\boldsymbol{\tau}_p^p$, $\mathbf{u}_{\text{dist}} = \boldsymbol{\omega}_p^{pd} + \mathbf{K}_1\mathbf{S}$, $\mathbf{K}_1 = \mathbf{K}_1^T > 0$, and $\mathbf{S} = -\mathcal{P}_a(\mathbf{C}_{pd})^V$. The attitude controller is defined as¹⁸

$$\begin{aligned} \boldsymbol{\nu}_1 &= \boldsymbol{\omega}_p^\times (\mathbf{J}_p^{\mathcal{B}c}\boldsymbol{\omega}_p + \mathbf{J}_s\dot{\boldsymbol{\gamma}}) - \mathbf{J}_p^{\mathcal{B}c} (\mathbf{K}_1\dot{\mathbf{S}} + \boldsymbol{\omega}_p^{pd \times} \boldsymbol{\omega}_p^{pd}), \\ \boldsymbol{\nu}_2 &= -\hat{\boldsymbol{\tau}}_p^p, \\ \boldsymbol{\nu}_3 &= -\mathbf{K}_\nu (\boldsymbol{\omega}_p^{pd} + \mathbf{K}_1\mathbf{S}) - \mathbf{K}_p\mathbf{S}, \end{aligned}$$

where $\mathbf{K}_\nu = \mathbf{K}_\nu^T > 0$, $\mathbf{K}_p = \mathbf{K}_p^T > 0$, and the attitude control input is $\boldsymbol{\eta} = -\mathbf{J}_s^{-1}(\boldsymbol{\nu}_1 + \boldsymbol{\nu}_2 + \boldsymbol{\nu}_3)$. Further details on the design and tuning of the controller can be found in Ref. 18.

B. Closed-Loop Linearized Model

The MPC policy prediction model relies on a linearization of the spacecraft dynamics in closed-loop with the inner-loop attitude controller about a nominal circular orbit with mean motion n , a nadir-pointing attitude, zero reaction wheel speeds, and zero observer states. The closed-loop linearized equations of motion are

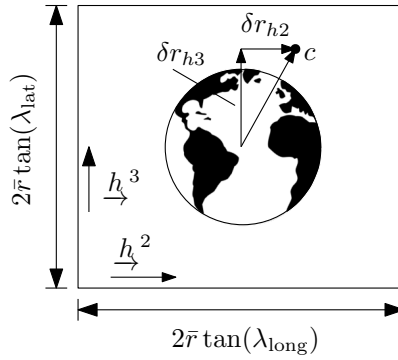


Figure 3. Illustration of the station keeping window described by $-\bar{r} \tan(\lambda_{\text{long}}) \leq \delta r_{h2} \leq \bar{r} \tan(\lambda_{\text{long}})$ and $-\bar{r} \tan(\lambda_{\text{lat}}) \leq \delta r_{h3} \leq \bar{r} \tan(\lambda_{\text{lat}})$, with the view looking in the $-\underline{h}^1$ direction towards Earth. The point c denotes the spacecraft's center of mass.

given by^{12, 13}

$$\begin{aligned}
\delta \ddot{\mathbf{r}}_h &= -2\bar{\omega}_p^\times \delta \dot{\mathbf{r}}_h - \Omega \delta \mathbf{r}_h + \mathbf{a}_h^p + \frac{1}{m_B} \mathbf{C}_{dh}^\top \mathbf{f}_p^{\text{thrust}}, \\
\delta \dot{\boldsymbol{\theta}} &= -\omega_0^\times \delta \boldsymbol{\theta} + \delta \boldsymbol{\omega} \\
\delta \dot{\boldsymbol{\omega}} &= \left(\mathbf{K}_1 \bar{\omega}_p^\times - (\bar{\omega}_p^\times)^2 + \mathbf{J}_p^{\mathcal{B}c^{-1}} (\mathbf{K}_\nu \bar{\omega}_p^\times - \mathbf{K}) \right) \delta \boldsymbol{\theta} + \boldsymbol{\tau}_p^{\text{thrust}} + \left(-\mathbf{K}_1 + \bar{\omega}_p^\times - \mathbf{J}_p^{\mathcal{B}c^{-1}} \mathbf{K}_\nu \right) \delta \boldsymbol{\omega} - \mathbf{J}_p^{\mathcal{B}c^{-1}} \mathbf{C}_{\text{dist}} \tilde{\mathbf{x}}_{\text{dist}}, \\
\ddot{\boldsymbol{\gamma}} &= \boldsymbol{\eta}, \\
\dot{\tilde{\mathbf{x}}} &= \mathbf{A}_{\text{dist}} \tilde{\mathbf{x}}_{\text{dist}} + \mathbf{B}_{\text{dist}} \delta \boldsymbol{\omega} + \mathbf{B}_{\text{dist}} (\mathbf{K}_1 - \bar{\omega}_p^\times) \delta \boldsymbol{\theta},
\end{aligned} \tag{2}$$

where $\bar{\omega}_p^\top = [0 \ 0 \ n]$, $\mathbf{C}_{pd} = \mathbf{C}_{pg} \mathbf{C}_{dg}^\top$ is the attitude error between \mathbf{C}_{pg} and the desired nadir-pointing orientation \mathbf{C}_{dg} , \mathbf{C}_{pg} is parameterized by a 3-2-1 Euler angle sequence with angles $\delta \boldsymbol{\theta}^\top = [\delta \phi \ \delta \theta \ \delta \psi]$, $\mathbf{K} = \mathbf{K}_\nu \mathbf{K}_1 + \mathbf{K}_p$, and $\Omega = \text{diag}\{-3n^2, 0, n^2\}$. Further details on this linearization are found in Refs. 12, 13. The closed-loop linearized model is written in state-space form as $\dot{\mathbf{x}} = \mathbf{A} \mathbf{x} + \mathbf{B} \mathbf{u} + \mathbf{B}_w \mathbf{w}$, where $\mathbf{x}^\top = [\delta \mathbf{r}^\top \ \delta \dot{\mathbf{r}}^\top \ \delta \boldsymbol{\theta}^\top \ \delta \boldsymbol{\omega}^\top \ \dot{\boldsymbol{\gamma}}^\top \ \tilde{\mathbf{x}}_{\text{dist}}^\top]$, $\mathbf{u}^\top = [\mathbf{f}_p^{\text{thrust}\top} \ \boldsymbol{\tau}_p^{\text{thrust}\top}]$, and $\mathbf{w}^\top = [\mathbf{a}_h^{p\top} \ \mathbf{0} \ \mathbf{0} \ \mathbf{0} \ \mathbf{0}]$. The discrete-time form of the closed-loop linearized model with time step Δt is $\mathbf{x}_{k+1} = \mathbf{A}_d \mathbf{x}_k + \mathbf{B}_d \mathbf{u}_k + \mathbf{B}_{w,d} \mathbf{w}_k$.

C. MPC Input and State Constraints

The magnitude of the control input $\mathbf{u}^\top = [\mathbf{f}_p^{\text{thrust}\top} \ \boldsymbol{\tau}_p^{\text{thrust}\top}]$ is constrained to satisfy $\mathbf{u}_{\min} \leq \mathbf{u} \leq \mathbf{u}_{\max}$, where $\mathbf{u}_{\max} = [\mathbf{f}_{\max}^{\text{thrust}\top} \ \boldsymbol{\tau}_{\max}^{\text{thrust}\top}]$ and $\mathbf{u}_{\min} = [\mathbf{f}_{\min}^{\text{thrust}\top} \ \boldsymbol{\tau}_{\min}^{\text{thrust}\top}]$. The maximum and minimum allowable forces and torques are chosen as $\mathbf{f}_{\max}^{\text{thrust}\top} = f_{\max}[1 \ 1 \ 1]$, $\mathbf{f}_{\min}^{\text{thrust}\top} = -f_{\max}[0 \ 1 \ 1]$, $\boldsymbol{\tau}_{\max}^{\text{thrust}\top} = -\boldsymbol{\tau}_{\min}^{\text{thrust}\top} = \tau_{\max}[1 \ 1 \ 1]$. The zero in $\mathbf{f}_{\min}^{\text{thrust}\top}$ is included to force the net thrust force acting on the satellite to act in the anti-nadir direction, which aids in the control allocation stage, where the gimballed booms feature the same directional constraint.

Two state constraints are included in the MPC policy based on the prescribed station keeping window and the maximum allowable attitude error. The station keeping window constraint is given by $\delta \bar{\mathbf{r}}_{\min} \leq \delta \bar{\mathbf{r}} \leq \delta \bar{\mathbf{r}}_{\max}$, where $\delta \bar{\mathbf{r}}_{\max}^\top = [\infty \ \bar{r} \tan(\lambda_{\text{long}}) \ \bar{r} \tan(\lambda_{\text{lat}})]$, $\delta \bar{\mathbf{r}}_{\min} = -\delta \bar{\mathbf{r}}_{\max}$, $\bar{r} = \|\bar{\mathbf{r}}_g\|$, and λ_{long} and λ_{lat} are the maximum deviations in longitude and latitude, respectively, that define the station keeping window [19, Ch. 5]. The constraint on attitude error is written as $\delta \boldsymbol{\theta}_{\min} \leq \delta \boldsymbol{\theta} \leq \delta \boldsymbol{\theta}_{\max}$.

D. Split-Horizon MPC Policy

Consider the split-horizon MPC policy^{14, 15} stated as

$$\min_{\mathcal{U}_t} \mathbf{x}_{N_1|t}^\top \mathbf{P}_1 \mathbf{x}_{N_1|t} + \sum_{k=0}^{N_1-1} \left(\mathbf{x}_{k|t}^\top \mathbf{Q} \mathbf{x}_{k|t} + \mathbf{u}_{k|t}^\top \mathbf{R} \mathbf{u}_{k|t} \right) + \mathbf{x}_{N_2|t}^\top \mathbf{P}_2 \mathbf{x}_{N_2|t} + \sum_{k=N_1}^{N_2-1} \left(\mathbf{x}_{k|t}^\top \mathbf{Q}_2 \mathbf{x}_{k|t} + \mathbf{u}_{k|t}^\top \mathbf{R} \mathbf{u}_{k|t} \right), \tag{3}$$

subject to

$$\begin{aligned}
\mathbf{x}_{k+1|t} &= \mathbf{A}_d \mathbf{x}_{k|t} + \mathbf{B}_d \mathbf{u}_{k|t} + \mathbf{B}_{w,d} \mathbf{w}_{k|t}, \\
\mathbf{x}_{0|t} &= \mathbf{x}(t), \quad \mathbf{w}_{k|t} = \hat{\mathbf{w}}_t(t+k), \\
\mathbf{x}_{\min} &\leq \mathbf{x}_{k|t} \leq \mathbf{x}_{\max}, \quad 0 \leq k \leq N_1, \\
\mathbf{x}_{\min,2} &\leq \mathbf{x}_{k|t} \leq \mathbf{x}_{\max,2}, \quad N_1 < k \leq N_2, \\
\mathbf{u}_{\min} &\leq \mathbf{u}_{k|t} \leq \mathbf{u}_{\max},
\end{aligned}$$

where N_1 is the prediction horizon of the states δr_{h3}^{cw} and $\delta \dot{r}_{h3}^{cw}$, N_2 is the prediction horizon of the remaining states, $\mathcal{U}_t = \{\mathbf{u}_{0|t}, \dots, \mathbf{u}_{N_2-1|t}\}$, $\mathbf{Q} = \mathbf{Q}^T \geq 0$ and $\mathbf{R} = \mathbf{R}^T > 0$ are constant state and control weighting matrices, $\mathbf{Q}_2 = \mathbf{Q}_2^T \geq 0$ is a modified state weighting matrix, and $\hat{\mathbf{w}}_i(j)$ is the open-loop predicted disturbance column matrix at time j based on data at time i . The matrices \mathbf{P}_1 and \mathbf{P}_2 are constructed from the matrix $\mathbf{P} = \mathbf{P}^T > 0$, which is the solution to the Discrete Algebraic Riccati Equation (DARE). Further details on \mathbf{Q}_2 , \mathbf{P}_1 , \mathbf{P}_2 , $\mathbf{x}_{\min,2}$, and $\mathbf{x}_{\max,2}$, can be found in the split-horizon MPC policy sections of Refs. 14, 15.

The control input at time t is $\mathbf{u}_{\text{mpc}}(t) = \mathbf{u}_{0|t}^*$, where \mathcal{U}_t^* is the minimizer of (3). This control input corresponds to the optimal body force and torque that serve as the inputs to the control allocation scheme described in Section IV-A.

IV. Control Allocation and Quantization

This section presents the main contributions of the paper, which are related to the allocation and quantization of the control input calculated using the split-horizon MPC policy formulated in Section III.

A. Control Allocation

Control allocation is concerned with allocating for suitable gimballed angles and thrust magnitudes of the North and South thruster booms, $\mathbf{z}_{\text{alloc}}^T = [\boldsymbol{\theta}^{N^T} \ \boldsymbol{\theta}^{S^T} \ f^N \ f^S]$, at each time period, given the optimal control force and torque inputs determined by the split-horizon MPC policy, \mathbf{u}_{mpc} . Allocation only occurs if the magnitude of $\mathbf{u}_{\text{mpc}}(t)$ is greater than the threshold $\epsilon_{\text{alloc}} > 0$. Below this threshold, no control allocation is performed and both thrusters remain off for the duration of the time step.

The objective of the allocation method is to minimize a weighted difference between the net force and torque produced by the chosen gimballed angles and thrust magnitudes, $\mathbf{u}_{\text{alloc}}(\mathbf{z}_{\text{alloc}})$, and \mathbf{u}_{mpc} , with an additional penalty on the thrust magnitudes. Mathematically, the control allocation problem is stated as

$$\min_{\mathbf{z}_{\text{alloc}}} (\mathbf{u}_{\text{mpc}} - \mathbf{u}_{\text{alloc}}(\mathbf{z}_{\text{alloc}}))^T \mathbf{W}_{\text{alloc}} (\mathbf{u}_{\text{mpc}} - \mathbf{u}_{\text{alloc}}(\mathbf{z}_{\text{alloc}})) + W_f (f^{N^2} + f^{S^2}), \quad (4)$$

subject to

$$\boldsymbol{\theta}_{\min}^N \leq \boldsymbol{\theta}^N \leq \boldsymbol{\theta}_{\max}^N, \quad (5)$$

$$\boldsymbol{\theta}_{\min}^S \leq \boldsymbol{\theta}^S \leq \boldsymbol{\theta}_{\max}^S, \quad (6)$$

$$0 \leq f^N \leq f_{\max}^N, \quad (7)$$

$$0 \leq f^S \leq f_{\max}^S, \quad (8)$$

$$0 \leq \mathbf{1}_1^T \mathbf{f}_p^{\text{thrust},N}(\boldsymbol{\theta}^N, f^N), \quad (9)$$

$$0 \leq \mathbf{1}_1^T \mathbf{f}_p^{\text{thrust},S}(\boldsymbol{\theta}^S, f^S), \quad (10)$$

$$0 \leq \mathbf{1}_1^T \mathbf{r}_p^{Nc}(\boldsymbol{\theta}^N), \quad (11)$$

$$0 \leq \mathbf{1}_1^T \mathbf{r}_p^{Sc}(\boldsymbol{\theta}^S), \quad (12)$$

where $\mathbf{W}_{\text{alloc}} = \mathbf{W}_{\text{alloc}}^T > 0$ and $W_f > 0$ are tuning weights, and

$$\mathbf{u}_{\text{alloc}}(\mathbf{z}_{\text{alloc}}) = \begin{bmatrix} \mathbf{f}_p^{\text{thrust},N}(\boldsymbol{\theta}^N, f^N) + \mathbf{f}_p^{\text{thrust},S}(\boldsymbol{\theta}^S, f^S) \\ \mathbf{r}_p^{Nc \times}(\boldsymbol{\theta}^N) \mathbf{f}_p^{\text{thrust},N}(\boldsymbol{\theta}^N, f^N) + \mathbf{r}_p^{Sc \times}(\boldsymbol{\theta}^S) \mathbf{f}_p^{\text{thrust},S}(\boldsymbol{\theta}^S, f^S) \end{bmatrix}$$

is the total force and torque acting on the spacecraft bus with the allocated gimballed angles and thrust magnitudes. Given that 10 values (8 gimballed angles and 2 thrust magnitudes) are allocated to match 6

control inputs (3 forces and 3 torques), the parameters $\mathbf{W}_{\text{alloc}}$ and W_f are used to tune the over-parameterized allocation process. Adjusting the value of $\mathbf{W}_{\text{alloc}}$ weights the relative importance of matching the forces and torques acting on the satellite in each axis. The tuning parameter W_f provides a means penalize thrust magnitude.

Constraints (5) and (6) ensure that the gimbals angles stay within prescribed limits (e.g., $\theta_i^N, \theta_i^S \in [-\pi, \pi]$), constraints (7) and (8) limit the allowable thrust magnitudes, constraints (9) and (10) restrict the force generated by each thruster to have a positive component in the anti-nadir direction, and constraints (11) and (12) make sure that the ends of the thruster booms remain on the anti-nadir side of the spacecraft. Constraints (9) and (10) can be substituted or augmented with other thrust direction constraints, such as constraints to avoid plume impingement.

The minimizer to the nonlinear optimization problem is given by $\mathbf{z}_{\text{alloc}}^*$, yielding an optimally-allocated force and torque of $\mathbf{u}_{\text{alloc}}^* = \mathbf{u}_{\text{alloc}}(\mathbf{z}_{\text{alloc}}^*)$.

B. Thruster Quantization

Quantization of the allocated force and torque is performed using an approach similar to the single-pulse quantization in Ref. 15, which solves for the on-off times of each thruster that minimize the predicted error in the system states induced by quantization at t_f , the end of the current time step. The quantization approach in this paper fixes the gimbals angles at the optimal values solved for in the allocation stage, which fixes the thrust direction. Quantization of each individual thruster only occurs when the magnitude of f^{N^*} or f^{S^*} is larger than a specified threshold $\epsilon_{\text{quant}} > 0$. No quantization is performed and the thruster remains off for the duration of the time step if the magnitude falls below the threshold. There typically exists a suitable range of ϵ_{quant} that results in both low Δv and a small number of on-off thruster cycles, which is discussed and studied for the case of the similar single-pulse quantization scheme in Ref. 15.

The predicted states of the system at time t_f based on the allocated thrust inputs are given by

$$\mathbf{x}_{\text{alloc}}(t_f) = e^{\mathbf{A}\Delta t}\mathbf{x}(t_0) + \mathbf{B}_d\mathbf{u}_{\text{alloc}}^*,$$

where $\mathbf{B}_d = \int_{t_0}^{t_f} e^{\mathbf{A}(t_f-\tau)}\mathbf{B}$. The predicted states of the system at time t_f based on the quantized thrust inputs are given by

$$\begin{aligned} \mathbf{x}_{\text{quant}}(t_f) = & e^{\mathbf{A}\Delta t}\mathbf{x}(t_0) + e^{\mathbf{A}(t_f-t_{2,N})}\mathbf{B}_d(t_{1,N}, t_{2,N})\mathbf{u}_{\text{alloc}}(\boldsymbol{\theta}^{N^*}, \boldsymbol{\theta}^{S^*}, f_{\text{max}}^N, 0) \\ & + e^{\mathbf{A}(t_f-t_{2,S})}\mathbf{B}_d(t_{1,S}, t_{2,S})\mathbf{u}_{\text{alloc}}(\boldsymbol{\theta}^{N^*}, \boldsymbol{\theta}^{S^*}, 0, f_{\text{max}}^S), \end{aligned}$$

where $\mathbf{B}_d(t_1, t_2) = \int_{t_1}^{t_2} e^{\mathbf{A}(t_2-\tau)}\mathbf{B}$, and $\mathbf{t}_N = \begin{bmatrix} t_{1,N} \\ t_{2,N} \end{bmatrix}$, $\mathbf{t}_S = \begin{bmatrix} t_{1,S} \\ t_{2,S} \end{bmatrix}$ define the on and off times of the North and South thrusters, respectively. The error between the two predicted states at t_f is given by

$$\begin{aligned} \mathbf{e} = & \mathbf{x}_{\text{alloc}}(t_f) - \mathbf{x}_{\text{quant}}(t_f) \\ = & \mathbf{B}_d\mathbf{u}_{\text{alloc}}^* - e^{\mathbf{A}(t_f-t_{2,N})}\mathbf{B}_d(t_{1,N}, t_{2,N})\mathbf{u}_{\text{alloc}}(\boldsymbol{\theta}^{N^*}, \boldsymbol{\theta}^{S^*}, f_{\text{max}}^N, 0) \\ & - e^{\mathbf{A}(t_f-t_{2,S})}\mathbf{B}_d(t_{1,S}, t_{2,S})\mathbf{u}_{\text{alloc}}(\boldsymbol{\theta}^{N^*}, \boldsymbol{\theta}^{S^*}, 0, f_{\text{max}}^S). \end{aligned}$$

Quantization is performed by solving $\min_{\mathbf{t}_N, \mathbf{t}_S} \mathbf{e}^T \mathbf{W}_{\text{quant}} \mathbf{e}$, subject to

$$\mathbf{A}_t \mathbf{t}_N \leq \mathbf{b}_t, \tag{13}$$

$$\mathbf{A}_t \mathbf{t}_S \leq \mathbf{b}_t, \tag{14}$$

where $\mathbf{W}_{\text{quant}} = \mathbf{W}_{\text{quant}}^T > 0$, $\mathbf{A}_t = \begin{bmatrix} 1 & -1 \\ -1 & 0 \\ 0 & 1 \end{bmatrix}$, and $\mathbf{b}_t = \begin{bmatrix} 0 \\ -t_0 \\ t_f \end{bmatrix}$. The constraints in (13) and (14) ensure

that the on and off times of each thruster are sequential and fall within the current time step. The parameter $\mathbf{W}_{\text{quant}}$ is used to tune the quantization problem by weighting the importance of minimizing error in each state.

The minimizer to the quantization problem is given by the on-off times \mathbf{t}_N^* and \mathbf{t}_S^* , which results in a control force and torque at time t of $\mathbf{u}(t) = \mathbf{u}_N(t) + \mathbf{u}_S(t)$, where

$$\mathbf{u}_N(t) = \begin{cases} \mathbf{u}_{\text{alloc}}(\boldsymbol{\theta}^{N^*}, \boldsymbol{\theta}^{S^*}, f_{\text{max}}^N, 0) & t_{1,N}^* \leq t \leq t_{2,N}^* \\ \mathbf{0} & t < t_{1,N}^* \text{ or } t_{2,N}^* < t, \end{cases}$$

$$\mathbf{u}_S(t) = \begin{cases} \mathbf{u}_{\text{alloc}}(\boldsymbol{\theta}^{N^*}, \boldsymbol{\theta}^{S^*}, 0, f_{\text{max}}^S) & t_{1,S}^* \leq t \leq t_{2,S}^* \\ \mathbf{0} & t < t_{1,S}^* \text{ or } t_{2,S}^* < t. \end{cases}$$

V. Simulation Results

In this section, the allocated and quantized MPC policy formulated in Sections III and IV is implemented in simulation. A spacecraft orbiting the Earth in a geostationary orbit is considered, with a mass of 4000 kg, and reaction wheels each with a mass of 10 kg, a radius of 0.2 m, and a thickness of 0.05 m. The spacecraft bus has dimensions of 1.6 m in the \underline{p}^1 direction, 0.92 m in the \underline{p}^2 direction, and 0.76 m in the \underline{p}^3 direction. Each thruster boom has a length of 1.7 m, the maximum thruster magnitude is $f_{\text{max}}^N = f_{\text{max}}^S = 0.14$ N, and the allowable gimbal angle ranges are defined by $\boldsymbol{\theta}_{\text{max}}^N = \boldsymbol{\theta}_{\text{max}}^S = -\boldsymbol{\theta}_{\text{min}}^N = -\boldsymbol{\theta}_{\text{min}}^S = \pi$ rad.

The performance constraints considered in simulation include a station keeping window of $\pm 0.05^\circ$ in both latitude and longitude, and a maximum allowable attitude error of $\pm 0.2^\circ$ in yaw, pitch, and roll. Simulations are performed for 425 orbits beginning at an epoch of Jan. 1, 2000, but only results from the last 365 orbits are presented and used for analysis, in an effort to remove any transient behavior. The maximum allowable angular momentum stored in the reaction wheels is 1000 N·m·s.

The MPC policy uses a split prediction horizon with $N_1 = 5$ hours, $N_2 = 20$ hours, a discretization time step of $\Delta t = 1$ hour, and weighting matrices of $\mathbf{Q} = \text{diag}\{\mathbf{Q}_r, \mathbf{Q}_{\dot{r}}, \mathbf{Q}_\theta, \mathbf{Q}_\omega, \mathbf{Q}_{\dot{\gamma}}, \mathbf{Q}_{\ddot{x}_{\text{dist}}}\}$ and $\mathbf{R} = \text{diag}\{\mathbf{R}_f, \mathbf{R}_\tau\}$, where $\mathbf{Q}_r = 10^{-9} \cdot \text{diag}\{0, 1, 1\}$ 1/m², $\mathbf{Q}_{\dot{r}} = \mathbf{0}$ s²/m², $\mathbf{Q}_\theta = 10^{-3} \cdot \mathbf{1}$ 1/rad², $\mathbf{Q}_\omega = \mathbf{0}$ s²/rad², $\mathbf{Q}_{\dot{\gamma}} = \mathbf{1}$ s²/rad², $\mathbf{Q}_{\ddot{x}_{\text{dist}}} = \mathbf{0}$, $\mathbf{R}_f = 10^{10} \cdot \mathbf{1}$ 1/N², and $\mathbf{R}_\tau = 10^{12} \cdot \mathbf{1}$ 1/(N²·m²). The inner-loop attitude controller gains are $\mathbf{K}_1 = \mathbf{1}$ 1/s, $\mathbf{K}_p = 20 \cdot \mathbf{1}$ N·m, $\mathbf{K}_v = 500 \cdot \mathbf{1}$ N·m·s. The observer dynamics of the inner-loop attitude controller are chosen as $\mathbf{A}_{\text{dist}} = \text{diag}\{\bar{\mathbf{A}}_{\text{dist}}, \bar{\mathbf{A}}_{\text{dist}}, \bar{\mathbf{A}}_{\text{dist}}\}$ and $\mathbf{C}_{\text{dist}} = \text{diag}\{\bar{\mathbf{C}}_{\text{dist}}, \bar{\mathbf{C}}_{\text{dist}}, \bar{\mathbf{C}}_{\text{dist}}\}$, where $\bar{\mathbf{A}}_{\text{dist}} = \begin{bmatrix} -0.001 & -\omega_d^2 \\ 1 & -0.001 \end{bmatrix}$, $\omega_d = 2\pi$ rad/day, and $\bar{\mathbf{C}}_{\text{dist}} = [1 \ 0]$. The observer matrix $\bar{\mathbf{B}}_{\text{dist}}$ is given by $\bar{\mathbf{B}}_{\text{dist}} = \mathbf{P}_{\text{dist}}^{-1} \bar{\mathbf{C}}_{\text{dist}}^\top$, where $\mathbf{P}_{\text{dist}} = \mathbf{P}_{\text{dist}}^\top \geq 0$ satisfies the Lyapunov equation $\bar{\mathbf{A}}_{\text{dist}}^\top \mathbf{P}_{\text{dist}} + \mathbf{P}_{\text{dist}} \bar{\mathbf{A}}_{\text{dist}} = -\mathbf{Q}_{\text{dist}}$ with $\mathbf{Q}_{\text{dist}} = 10^{-3} \cdot \mathbf{1}$.

Three simulations are performed to highlight each individual aspect of the control policy. First, a simulation with only the split-horizon MPC policy is implemented assuming that an arbitrary force and torque can be applied to the satellite hub. This effectively assumes the satellite is equipped with 12 thrusters that can provide a force and torque in any direction, as in Ref. 11. Second, a simulation is performed with the split-horizon MPC policy and the control allocated to a set of gimbal angles and variable thruster magnitudes. Third, a simulation with the split-horizon MPC policy, control allocation, and thruster quantization is included. The last simulation is an indication of the control policy's performance with realistic electric thrusters, while the first two simulations illustrate the Δv accumulated at each stage of the control policy.

A. Simulation 1: Split-Horizon MPC Policy

A simulation is performed with only the split-horizon MPC policy (i.e., the control allocation and thruster quantization of Section IV is omitted), resulting in $\Delta v = 47.6$ m/s. Plots of the results are found in Figure 4, which show that the station keeping and attitude constraints are satisfied, and the angular momentum stored in the reaction wheels remains small. An annual Δv of 47.6 m/s is comparable to benchmark results with much less limited and more expensive thruster configurations.¹ These excellent results are in part due to having relaxed many of the propulsion system constraints, which are re-introduced in Simulations 2 and 3.

B. Simulation 2: Split-Horizon MPC Policy with Control Allocation

A simulation is performed with a non-quantized version of the proposed MPC policy (i.e., the quantization of Section IV-B is omitted). The control allocation method uses tuning values of $\mathbf{W}_{\text{alloc}} = \text{diag}\{\mathbf{W}_{\text{alloc},f}, \mathbf{W}_{\text{alloc},\tau}\}$

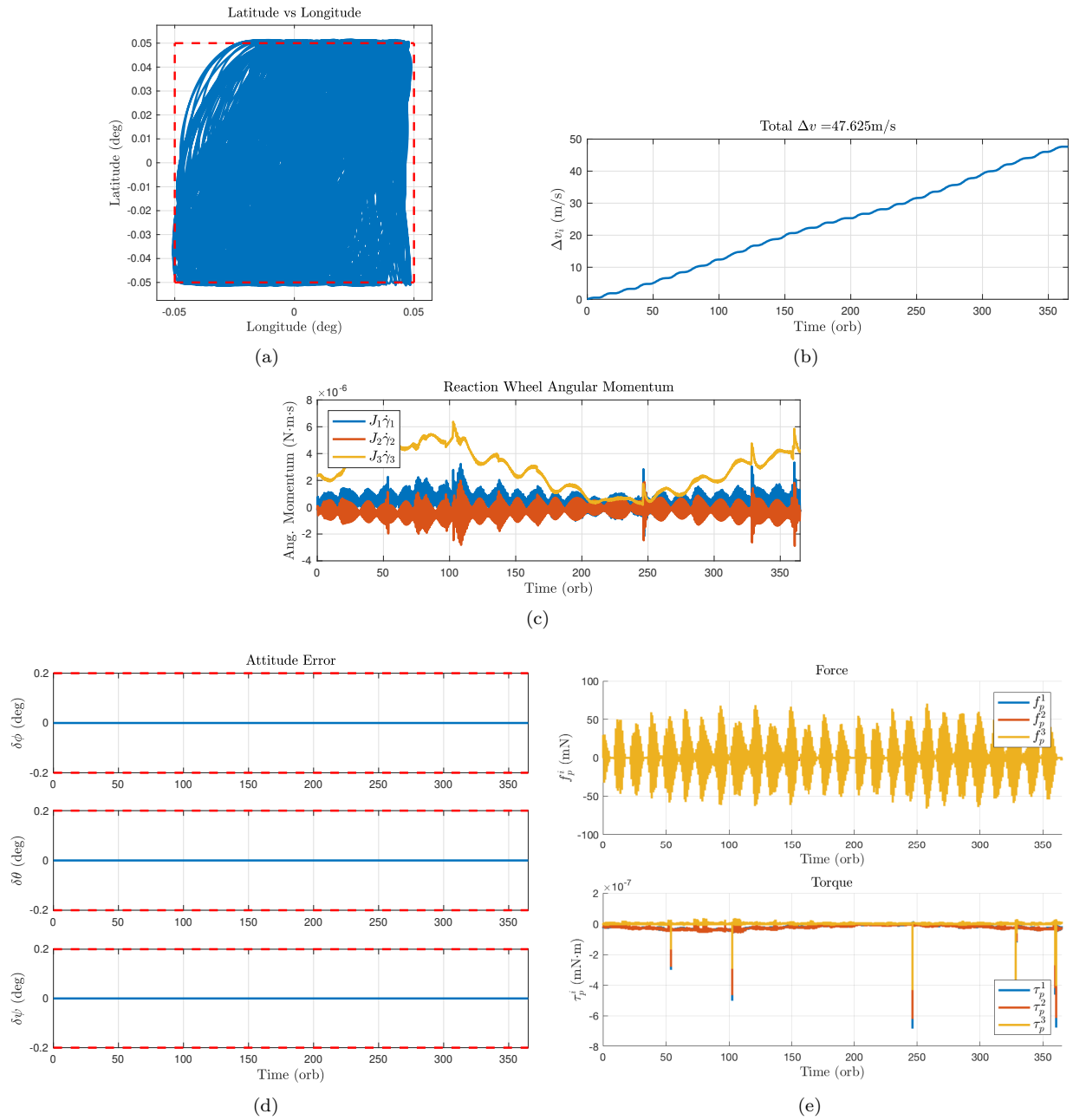


Figure 4. Simulation 1 results: one year simulation using the split-horizon MPC policy. Plots of (a) station keeping window, (b) accumulated Δv , (c) reaction wheel angular momentum, (d) spacecraft attitude error, and (e) applied body forces and torques.

and $W_f = 5 \times 10^{-2} \text{ 1/N}$, and a threshold of $\epsilon_{\text{alloc}} = 1 \times 10^{-3} \text{ mN}$, where $\mathbf{W}_{\text{alloc},f} = 5 \times 10^4 \cdot \mathbf{1} \text{ 1/N}^2$ and $\mathbf{W}_{\text{alloc},\tau} = 10^4 \cdot \mathbf{1} \text{ 1/(N}^2 \cdot \text{m}^2)$. Plots of the results are found in Figure 5, and the fuel consumption is $\Delta v = 53.5 \text{ m/s}$. The control allocation results in a 12.4 % increase in Δv compared to the unallocated results, minimal effect on attitude error, and additional angular momentum stored in the reaction wheels that is within the specified limits.

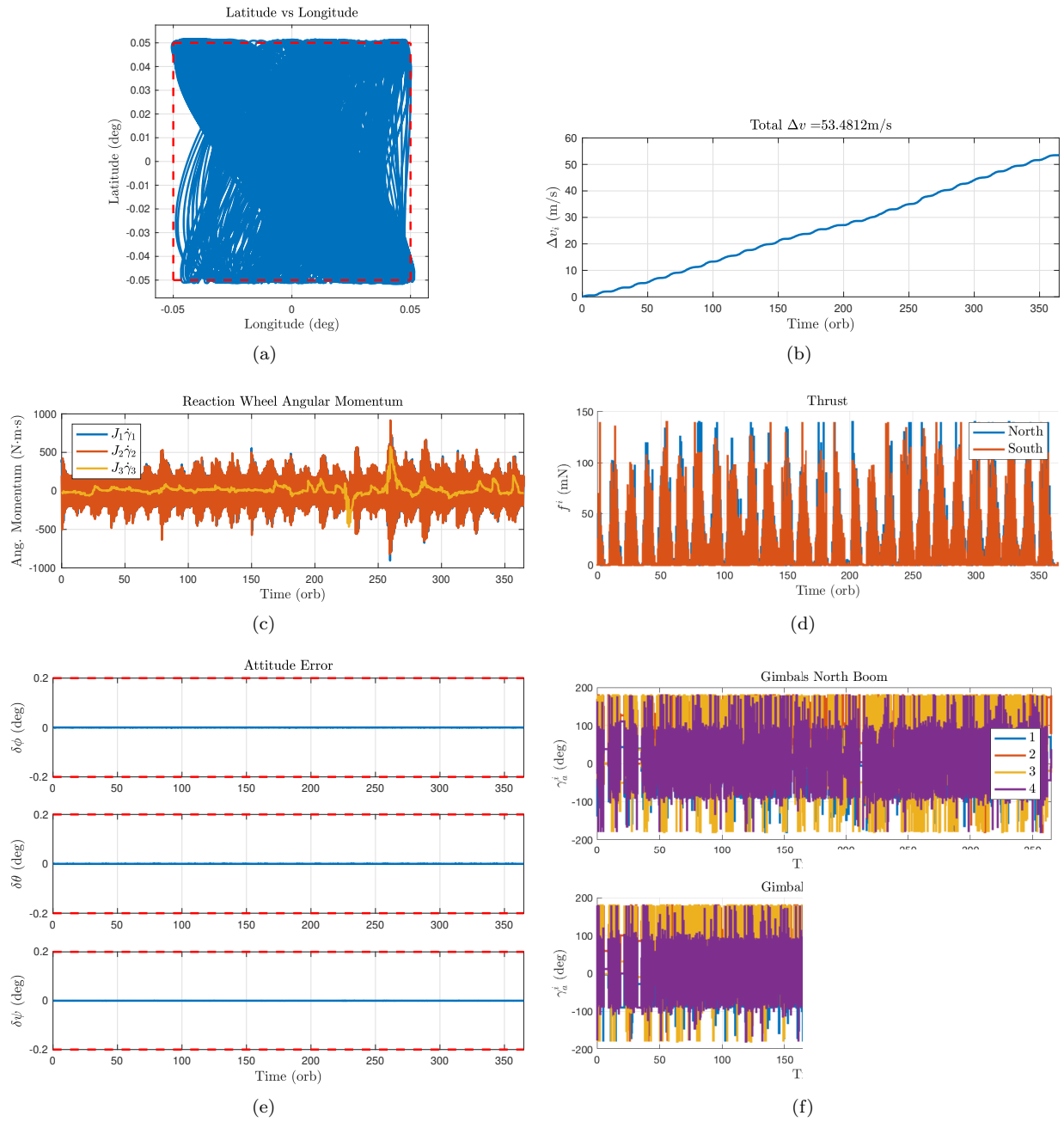


Figure 5. Simulation 2 results: one year simulation using the split-horizon MPC policy and control allocation. Plots of (a) station keeping window, (b) accumulated Δv , (c) reaction wheel angular momentum, (d) thruster magnitudes, (e) spacecraft attitude error, and (f) North and South boom gimbal angles.

C. Simulation 3: Split-Horizon MPC Policy with Control Allocation and Thruster Quantization

A simulation is performed with the complete MPC policy, including control allocation and thruster quantization. The thruster quantization method uses a tuning value of

$$\mathbf{W}_{\text{quant}} = \text{diag}\{\mathbf{W}_{\text{quant},\mathbf{r}}, \mathbf{W}_{\text{quant},\dot{\mathbf{r}}}, \mathbf{W}_{\text{quant},\boldsymbol{\theta}}, \mathbf{W}_{\text{quant},\boldsymbol{\omega}}, \mathbf{W}_{\text{quant},\dot{\boldsymbol{\gamma}}}, \mathbf{W}_{\text{quant},\bar{\mathbf{x}}_{\text{dist}}}\}$$

and a threshold of $\epsilon_{\text{quant}} = 2$ mN, where $\mathbf{W}_{\text{quant},\mathbf{r}} = 10^{-6} \cdot \mathbf{1}$ 1/m², $\mathbf{W}_{\text{quant},\dot{\mathbf{r}}} = 10^6 \cdot \mathbf{1}$ s²/m², $\mathbf{W}_{\text{quant},\boldsymbol{\theta}} = 10^2 \cdot \mathbf{1}$ 1/rad², $\mathbf{W}_{\text{quant},\boldsymbol{\omega}} = 10^6 \cdot \mathbf{1}$ s²/rad², $\mathbf{W}_{\text{quant},\dot{\boldsymbol{\gamma}}} = \mathbf{1}$ s²/rad², $\mathbf{W}_{\text{quant},\bar{\mathbf{x}}_{\text{dist}}} = \mathbf{1}$. Plots of the results are found

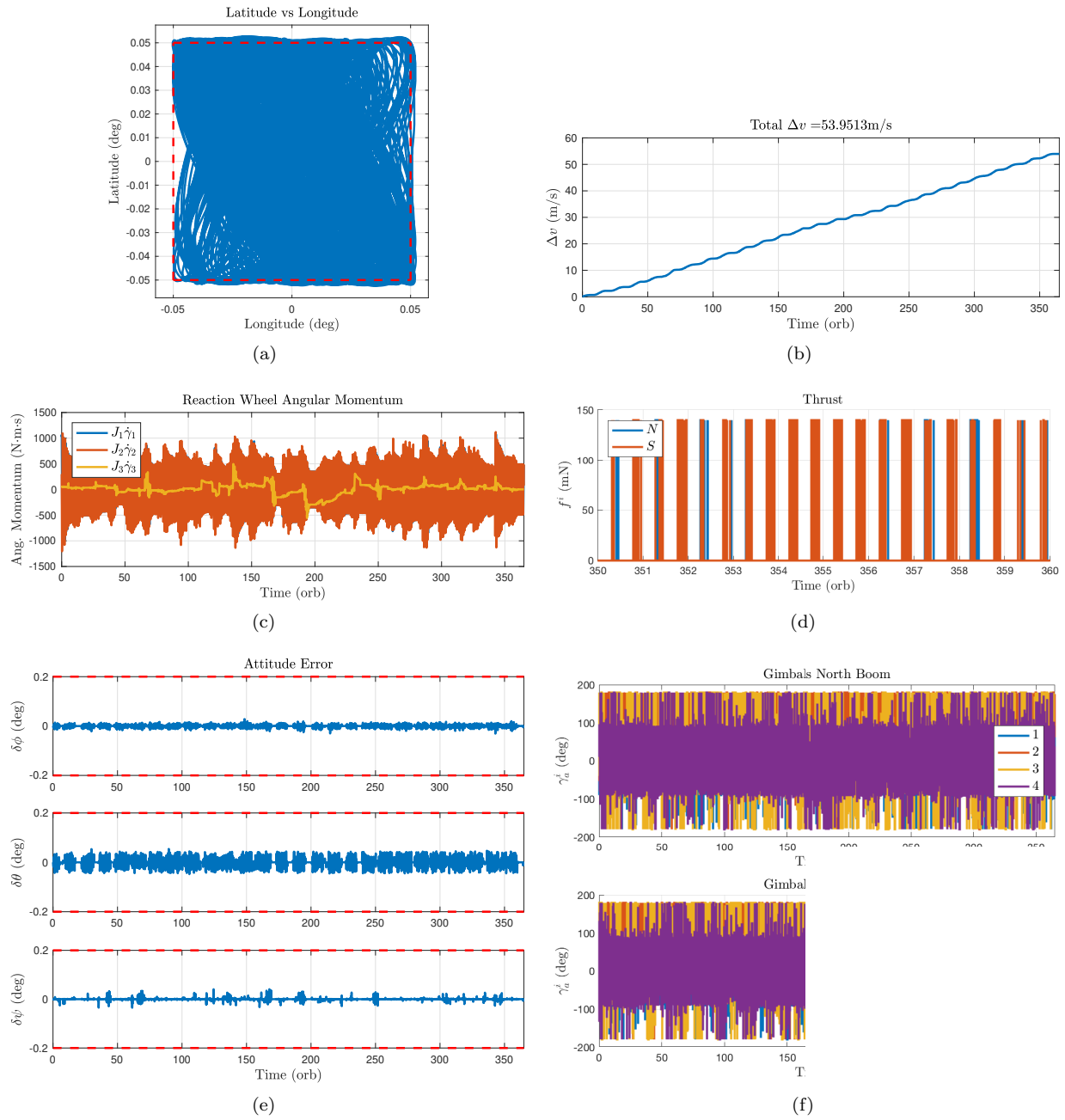


Figure 6. Simulation 3 results: one year simulation using the split-horizon MPC policy, control allocation, and thruster quantization. Plots of (a) station keeping window, (b) accumulated Δv , (c) reaction wheel angular momentum, (d) thruster magnitudes between orbits 350 and 360, (e) spacecraft attitude error, and (f) North and South boom gimbals angles.

in Figure 6, and the fuel consumption is $\Delta v = 53.9$ m/s with an average of 7.8 on-off cycles/thruster/orbit. This is a 13.2 % increase in Δv from the unallocated results of Simulation 1 and only a 0.75 % increase compared to the non-quantized result of Simulation 2. Figure 6 shows that the attitude error increases significantly compared to the previous results, but the angular momentum of the reaction wheels is managed.

D. Discussion of Results

The Δv consumed in each of the simulations is summarized in Table 1. The results demonstrate that control allocation does not result in a significant increase in Δv , which is due to the fact that the four thruster

Table 1. Δv for Simulations 1, 2, and 3.

| Simulation | Δv (m/s) |
|--|------------------|
| 1 - Split Horizon MPC | 47.6 |
| 2 - Split Horizon MPC w/ Control Allocation | 53.5 |
| 3 - Split Horizon MPC w/ Control Allocation and Quantization | 53.9 |

boom DOFs provide a sufficient range of thrust direction to match the force and torque generated by the split-horizon MPC policy prior to allocation. The thruster quantization stage results in a significant increase in Δv , however, we believe that with a careful tuning of the calibration parameters the fuel consumption can be further reduced. Even with the increase in Δv due to thrust quantization, the proposed control policy for the new thruster configuration is quite effective and satisfies all specification constraints in the numerical simulations.

VI. Conclusions

This paper introduced a split-horizon MPC policy for simultaneous station keeping, attitude control, and momentum management of a GEO satellite equipped with two thrusters mounted on gimballed booms with 4 DOFs, that includes control allocation and thrust quantization stages. A quadratic programming problem is first solved based on the split-horizon MPC policy, followed by control allocation and thrust quantization, which are both nonlinear optimization problems. This control policy determines optimal thruster boom gimballed angles and thruster on-off times that meet the physical constraints of the thruster-boom assembly.

Future work will focus on tuning the thruster quantization parameters to reduce fuel consumption and the number of on-off thruster cycles, analyzing closed-loop robustness to model uncertainty, and the inclusion of additional thrust direction constraints (e.g., constraints to avoid plume impingement).

References

- ¹Martinez-Sanchez, M. and Pollard, J. E., "Spacecraft electric propulsion – An overview," *Journal of Propulsion and Power*, Vol. 14, No. 5, 1998, pp. 688–699.
- ²Leomanni, M., Garulli, A., Giannitrapani, A., and Scortecchi, F., "All-Electric Spacecraft Precision Pointing using Model Predictive Control," *Journal of Guidance, Control, and Dynamics*, Vol. 38, No. 1, 2015, pp. 161–168.
- ³Leomanni, M., Rogers, E., and Gabriel, S. B., "Explicit Model Predictive Control Approach for Low-Thrust Spacecraft Proximity Operations," *Journal of Guidance, Control, and Dynamics*, Vol. 37, No. 6, 2014, pp. 1780–1790.
- ⁴Vazquez, R., Galivan, F., and Camacho, E. F., "Pulse-Width Predictive Control for LTV Systems with Application for Spacecraft Rendez-Vous," *Control Engineering Practice*, Vol. 60, March 2017, pp. 199–210.
- ⁵Gazzino, C., Louembet, C., Arzelier, D., Jozefowicz, N., Losa, D., Pittet, C., and Cerri, L., "Integer Programming for Optimal Control of Geostationary Station Keeping of Low-Thrust Satellites," LAAS Report 16341, July 2017.
- ⁶Gazzino, C., Arzelier, D., Cerri, L., Losa, D., Louembet, C., and Pittet, C., "Solving the Minimum-Fuel Low-Thrust Geostationary Station Keeping Problem via the Switching Systems Theory," *7th European Conference for Aeronautics and Space Sciences*, Milano, Italy, July 2017.
- ⁷Gazzino, C., Arzelier, D., Losa, D., Louembet, C., Pittet, C., and Cerri, L., "Optimal Control for Minimum-Fuel Geostationary Station Keeping of Satellites Equipped with Electric Propulsion," *IFAC Papers Online*, Vol. 49, No. 17, 2016, pp. 379–384.
- ⁸Gazzino, C., Arzelier, D., Louembet, C., Cerri, L., Pittet, C., and Losa, D., "Long-Term Electric-Propulsion Geostationary Station-Keeping via Integer Programming," *Journal of Guidance, Control, and Dynamics*, 2019.
- ⁹Gazzino, C., Arzelier, D., Cerri, L., Losa, D., Louembet, C., and Pittet, C., "A Three-Step Decomposition Method for Solving the Minimum-Fuel Geostationary Station Keeping of Satellites Equipped with Electric Propulsion," *Acta Astronautica*, 2019.
- ¹⁰Li, L., Zhang, J., Li, Y., and Zhao, S., "Geostationary Station-Keeping with Electric Propulsion in Full and Failure Modes," *Acta Astronautica*, 2019.
- ¹¹Weiss, A., Kalabić, U., and Di Cairano, S., "Model Predictive Control for Simultaneous Station Keeping and Momentum Management of Low-Thrust Satellites," *Proc. American Control Conference*, Chicago, IL, 2015, pp. 2305–2310.
- ¹²Walsh, A., Di Cairano, S., and Weiss, A., "MPC for Coupled Station Keeping, Attitude Control, and Momentum Management of Low-Thrust Geostationary Satellites," *Proc. American Control Conference*, Boston, MA, 2016, pp. 7408–7413.
- ¹³Zlotnik, D., Di Cairano, S., and Weiss, A., "MPC for Coupled Station Keeping, Attitude Control, and Momentum Management for GEO Satellites using On-Off Electric Propulsion," *Proc. IEEE Conference on Control Technology and Applications*, Kohala Coast, Hawai'i, 2017, pp. 1835–1840.

¹⁴Caverly, R. J., Di Cairano, S., and Weiss, A., “Split-Horizon MPC for Coupled Station Keeping, Attitude Control, and Momentum Management of GEO Satellites using On-Off Electric Propulsion,” *Proc. American Control Conference*, Milwaukee, WI, 2018, pp. 652–657.

¹⁵Caverly, R. J., Di Cairano, S., and Weiss, A., “Quantization of an MPC Policy for Coupled Station Keeping, Attitude Control, and Momentum Management of GEO Satellites,” *Proc. European Control Conference*, Limassol, Cyprus, 2018, pp. 3114–3119.

¹⁶Rawlings, J. B. and Mayne, D. Q., *Model predictive control: Theory and design*, Nob Hill Pub. Madison, Wisconsin, 2009.

¹⁷Sembély, X., Wartelski, M., Doubrère, P., Deltour, B., Cau, P., and Rochard, F., “Design and Development of an Electric Propulsion Deployable Arm for Airbus Eurostar E3000 ComSat Platform,” *Proc. 35th International Electric Propulsion Conference*, Atlanta, GA, 2017.

¹⁸Weiss, A., Kolmanovsky, I., Bernstein, D. S., and Sanyal, A., “Inertia-Free Spacecraft Attitude Control Using Reaction Wheels,” *Journal of Guidance, Control, and Dynamics*, Vol. 36, No. 5, 2013, pp. 1425–1439.

¹⁹Soop, E. M., *Handbook of Geostationary Orbits*, Springer, 1994.